# Palladium Nanoparticles Decorated Single-Walled Carbon Nanotube Hydrogen Sensor

**Syed Mubeen, Ting Zhang, Bongyoung Yoo, Marc A. Deshusses,* and Nosang V. Myung***

*Department of Chemical and Environmental Engineering and Center for Nanoscale Science and Engineering, University of California—Riverside, Riverside, California 92521*

*Received: November 20, 2006; In Final Form: February 5, 2007*

We developed a simple and cost-effective fabrication technique to construct a hydrogen nanosensor by decorating single-walled carbon nanotubes with Pd nanoparticles. By varying the sensor's synthesis conditions (e.g., Pd electrodeposition charge, deposition potential, and initial baseline resistance of the SWNT network), the sensing performance was optimized. The optimized sensor showed excellent sensing properties toward hydrogen ($\Delta R/R$ of 0.42%/ppm) with a lower detection limit of 100 ppm and a linear response up to 1000 ppm. The response time decreased from tens of minutes to a few minutes with increasing hydrogen concentration at room temperature. The sensor's recovery time improved under humid air conditions compared to dry air conditions.

## Introduction

There is increasing demand for hydrogen sensors in numerous applications such as chemical and petroleum refining, neon and xenon production, rocket fuels for spacecraft, fuel cells, semiconductor processing for microelectronics, and biomedical applications. Hydrogen in the breath is also a good indicator for various diseases, including lactose intolerance, fructose malabsorption, fibromyaligia, and neonatal necrotizing enterocolitis (NEC).[1] Hence, in view of these applications, a hydrogen sensor having good sensitivity, low detection limit, fast response, and recovery time, good specificity with low false positive and long-term stability with wide temperature operation range is required.[2]

Numerous approaches are being investigated to develop hydrogen sensors. Most commercially available hydrogen sensors are based on metal oxides (e.g., stannic oxide) films configured in chemiresistor mode. Typically, these metal oxide-based sensors must be heated usually over 400 °C in order to maintain proper operation.[3] Recently, Pd or Pd-based alloy thin and thick film-based sensors have been proposed as an alternative to metal oxide sensors as they show both a high sensitivity and selectivity towards hydrogen, and are able to detect hydrogen at near room temperature.[4] The ability of hydrogen atoms to occupy the octahedral interstitial positions within Pd's Face Centered Cubic (FCC) lattice structure forms the basis for these sensors. The incorporation of hydrogen atoms results in the formation of Pd hydride, leading to possible property changes (e.g., electrical resistance, work function, grain size, and $\alpha-\beta$ phase transition). Using the change in resistance of Pd upon exposure to hydrogen, thick film[5] based chemiresistors were developed. On the other hand, Lundström et al.[6] and Dwivedi et al.[7] developed hydrogen sensors based on Field Effect Transistor (FET) configuration with Pd film as the gate electrode.

Recently, one-dimensional nanostructures based chemical sensors have attracted a great deal of attention due to their small size, superior sensitivity, real-time detection with low-power consumption. In the case of hydrogen sensing, single Pd nanowire,[8] Pd meso-wires,[9] Pd evaporated on carbon nanotubes[10] and titanium dioxide nanotubes[11] have been investigated as sensing materials.

Carbon nanotubes (CNTs) have generated an enormous interest due to their fundamental behavior which could lead to a wide variety of new applications. CNTs can be either electrically conductive or semiconductive, depending on their helicity.[12] Further, since all carbon atoms in a single-walled carbon nanotube (SWNT) are exposed to the outer surface, SWNTs could be ideal building blocks for making gas sensors. Indeed, gas sensors made from semiconducting SWNTs showed good sensitivities toward $NH_3$ and $NO_2$ at room temperature.[13,14] This is a significant improvement over conventional sensors which usually require heating to temperatures exceeding 200 °C. However, bare SWNTs have not shown good sensitivity toward hydrogen due to their poor electronic interaction between these molecules. A likely method to overcome this drawback is to functionalize the nanotubes with nanoparticles made of a suitable material such as Pd or metal oxides.

In this report, we demonstrate site-specific electrodeposition of Pd nanoparticles on SWNT networks and show that the resulting SWNT networks have improved properties for hydrogen sensing. SWNT networks were selected over a single SWNT sensor, because SWNT networks have higher signal-to-noise ratio and ensure reproducible sensor performance.[15] Electrodeposition has several advantages over other functionalization methods including (1) simplicity and low-cost, (2) ambient operating conditions, (3) ability to "tailor" the materials properties (e.g., crystal orientation, grain size), (4) ability to deposit various materials including metals, metal oxides, semiconductors, and conducting polymers, (5) ability to control the properties of deposited materials such as size and density by simply altering the deposition parameters such as electrolyte composition, deposition time and potential, and (6) site-specific deposition, as shown by Fan et al.,[16] who demonstrated that a sequence of electrochemical potentials applied to a SWNT resulted in selective materials deposition at the defect sites. In the present paper, we demonstrate fabrication of a hydrogen nanosensor based on electrodeposited Pd nanoparticles on

* Corresponding authors. E-mails: myung@engr.ucr.edu and mdeshuss@engr.ucr.edu. Address: Department of Chemical and Environmental Engineering at University of California-Riverside, Bourns Hall, 900 University Avenue, Riverside, CA 92521.

10.1021/jp067716m CCC: $37.00 
Published on Web 04/11/2007

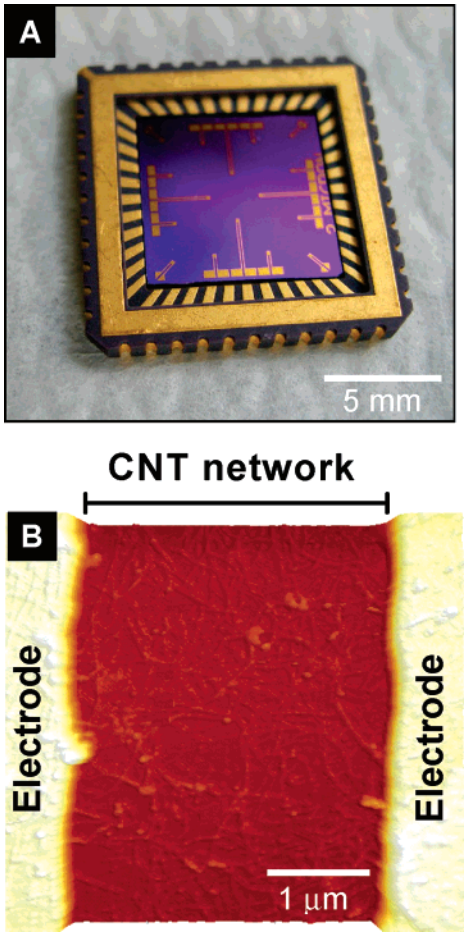


**Figure 1.** Optical image of 16 sensors array on chip carrier (A) and AFM image of SWNT network across microfabricated gold electrodes (B).

SWNTs. The sensor's synthesis conditions (deposition charge, deposition potential, baseline resistance of the SWNT network) were optimized to enhance hydrogen sensing performance. The technique described herein allows the spatial functionalization of nanostructures, enabling the creation of arrays of individually addressable high-density nanosensor arrays.

## Experimental

The electrodes for the sensors array were microfabricated on silicon substrate using standard lithographic patterning. Using chemical vapor deposition (CVD), one micron thick $SiO_2$ film was first deposited on a (100) oriented silicon wafer to insulate the substrate. After photo lithographically defining the electrode area, a Cr adhesion layer and a ~3000 Å-thick Au layer were e-beam evaporated. Finally, the electrodes were defined using lift-off techniques. The gap distance between electrodes was fixed at 3 $\mu$m. Figure 1 shows the optical and AFM images of sensors array.

The fabrication steps of the Pd nanoparticles decorated SWNTs hydrogen sensor are illustrated in Figure 2. First, SWNTs functionalized with −COOH group (Carbon Solution, Inc. Riverside, CA) were dispersed (0.5 $\mu$g/mL) in dimethyl formamide (DMF) using ultrasonic force. The amide group of DMF can attach to the surface of the nanotubes making it a suitable solvent for obtaining uniformly suspended SWNTs.[15] Then, a 0.05 $\mu$L drop of the SWNT suspension was deposited onto the electrode gap using a microsyringe (Figure 2A). After evaporation of the solution, a network of SWNTs bridged each

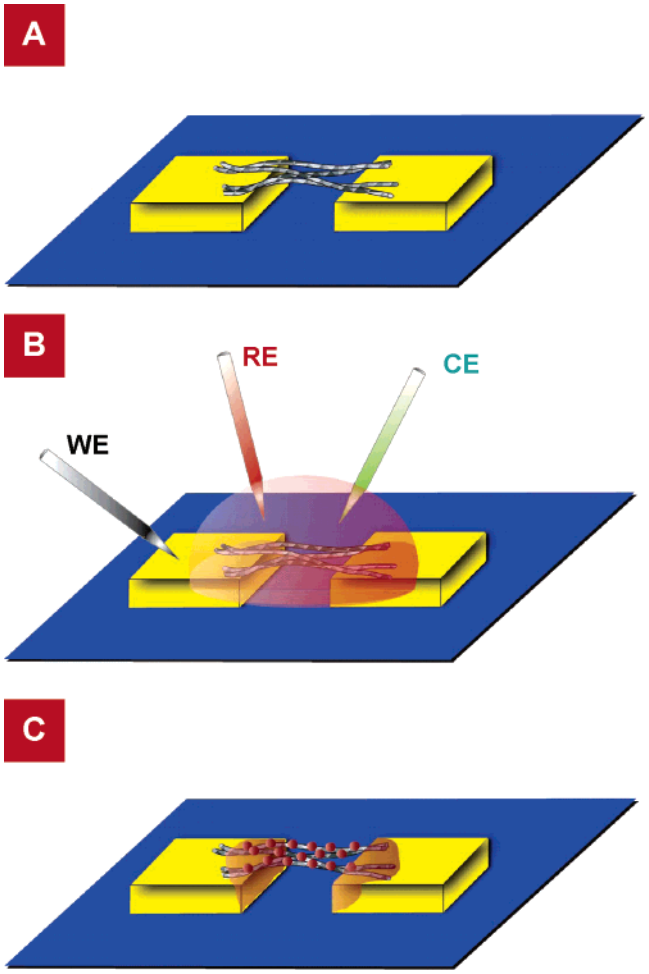


**Figure 2.** Schematic of the electrochemical synthesis method. (A) Nanotubes are deposited across the electrodes. (B) Electrochemical functionalization of the SWNTs: WE = working electrode; CE = counter electrode; RE = reference electrode. (C) Pd nanoparticles formed on SWNTs.

electrode gap (Figure 1B). The sensors were then annealed at 350 °C for 60 min under argon atmosphere to reduce the contact resistance between SWNTs and the gold electrodes and to remove any DMF residues present. The density of the SWNTs across the gap was adjusted by varying the concentration of the SWNTs in the DMF solution and the droplet size.

Pd nanoparticles decoration on SWNTs was performed using three electrode cell configurations as shown in Figure 2B. The electrochemical cell was formed by dropping a 3$\mu$L of Pd electrolyte solution on top the SWNT network, and platinum and Ag/AgCl wires were inserted into the electrolyte. The annealed SWNT network along with the gold electrodes served as the working electrode, while platinum wire and Ag/AgCl wire served as the counter electrode and reference electrode, respectively. The working electrode area was approximately 0.1 $cm^2$. The Pd electrolyte consisted of 10 g/L of Pd $(NH_2)_2(NO_2)_2$ and 100 g/L of ammonium sulfamate. The solution pH was adjusted to 8.0 by addition of sulfamic acid and sodium hydroxide. An alkaline electrolyte was selected to deposit Pd nanoparticles to prevent the dissolution of Cr adhesion layer which can be readily attacked in an acidic environment.[17] The potential across the working electrode was controlled by the use of Ag/AgCl reference electrode. The deposition was carried out at 25 °C and at ambient pressure. As the current conduction is through the nanotube networks, by applying a desired potential, the metal cation is reduced and deposited on the

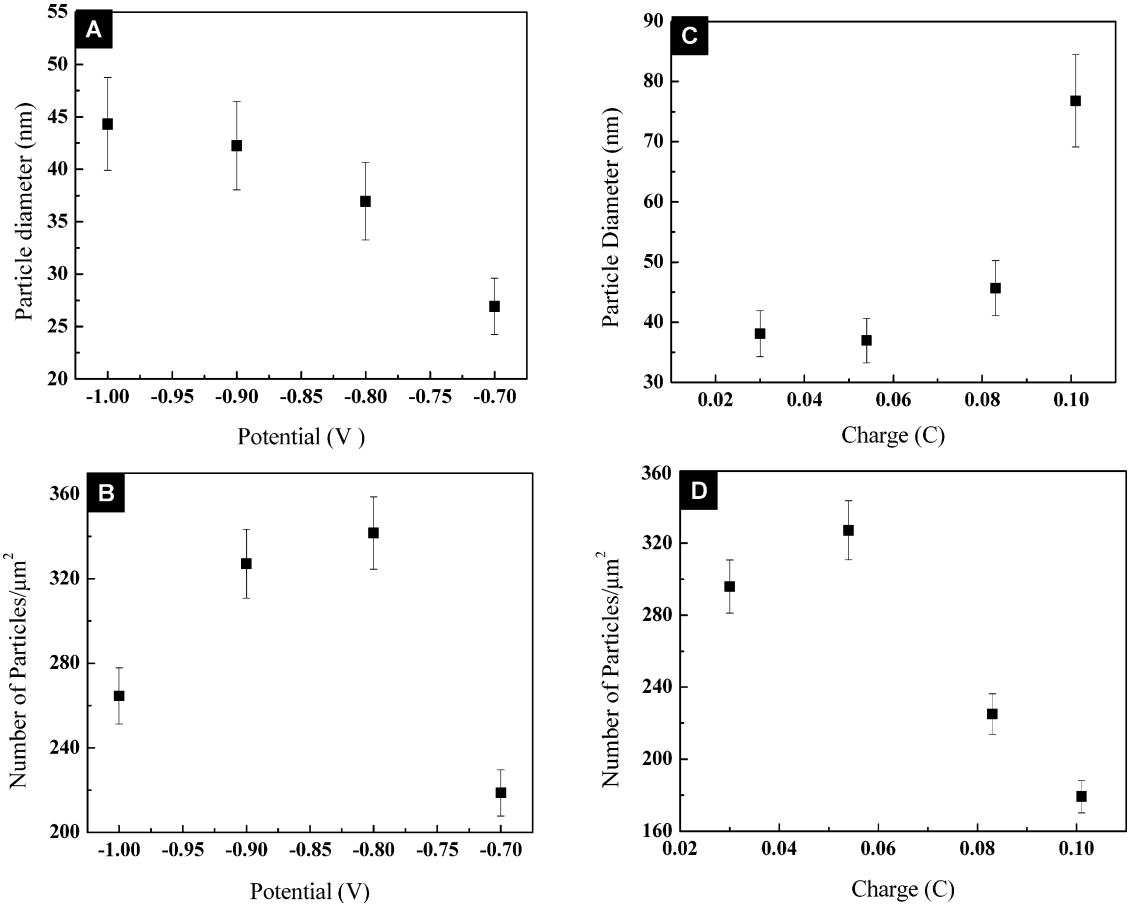


**Figure 3.** Variation of Pd particle diameter and density on SWNTs for different potentials (A and B) and for charges (C and D) applied.

cathode leaving all other devices on the chip unmodified. After deposition, the device was rinsed well with acetone and nanopure water in order to ensure that the substrate is free from contaminants from electrolyte solution. The effect of deposition charge and deposition potential on the size and number of the Pd nanoparticles on SWNTs were examined by varying the deposition potentials from −0.7 to −1.0 V vs Ag/AgCl and deposition charge from 0.03 to 0.10 C. The deposition area was fixed at 1 $cm^2$. Size and number of Pd nanoparticles on SWNTs were determined using scanning electron microscopy (Philips model # XL30-FEG) and atomic force microscopy (PSIA, Inc., Model # XE100). For calculating the particle diameter and density, 4 $\mu$m by 4 $\mu$m image (5 sets) were selected, and mean particle diameter and density of Pd on SWNT were calculated. The particle diameter and density of ultrafine Pd nanoparticles were not accurately measured due to limitations of SEM and AFM.

The temperature dependent electrical properties of SWNTs were characterized using a Physical Property Measurement System (PPMS). The effects of deposition time on I−V characteristic of Pd−SWNTs were analyzed using a semiconductor parameter analyzer (HP Model # 4155A).

For gas detection studies, the electrodes were wire-bonded and each sensor was connected in series with a load resistance. The value of the load resistance was chosen to be as close as possible to the initial resistance of the sensor to optimize the resolution obtained from the measurements. The circuit was subjected to a fixed voltage (1 V DC) and the electrical resistance of the sensor was determined by continuously monitoring the voltage over the load resistor and applying Ohm's law. A 3.6 $cm^3$ sealed glass chamber with gas inlet and outlet ports for gas flow-through was positioned over the sensor chip. All experiments were conducted with hydrogen (purity: 99.998%) diluted in humid air at a gas flow of 400 std. $cm^3$ $min^{-1}$. The humid air was obtained by bubbling dry air (purity: 99.998%) through a bubbler column. The hydrogen and humid air gas flow rates were regulated by mass flow controllers (Alicat Scientific Incorporated, Tucson, AZ). A custom Labview computer program was developed to continuously control and monitor the voltage of the circuit using Fieldpoint analog input and output modules (National Instruments, Austin, TX). In all experiments, the sensors were first exposed to air to obtain the baseline, then to a desired concentration of hydrogen gas, and then back to air which completed one cycle.

## Results and Discussions

To understand the effect of electrodeposition parameters such as potential and charge on the functionalization of SWNTs, systematic deposition of Pd nanoparticles was first carried out. Four different potentials from −0.7 to −1 V were selected to deposit palladium on SWNTs based on linear sweep voltammogram. For the same amount of charge passed, the number of Pd particles nucleated on SWNTs was highest at −0.8 V and the average particle diameter approximately increased 2-fold from −0.7 to −1.1 V (Figure 3A,B). The observed trend might be due to the hydrogen gas evolution which occurs at the most cathodic potentials leading to a reduced current efficiency of the system. Hence a lower deposition potential was selected (−0.8 V, in this case) for which we observed a higher Pd nanoparticle particle density with a small particle diameter. Charge-dependent studies were carried out at this potential. As pointed out by Fan et.al.,[16] at higher charge passed the particle

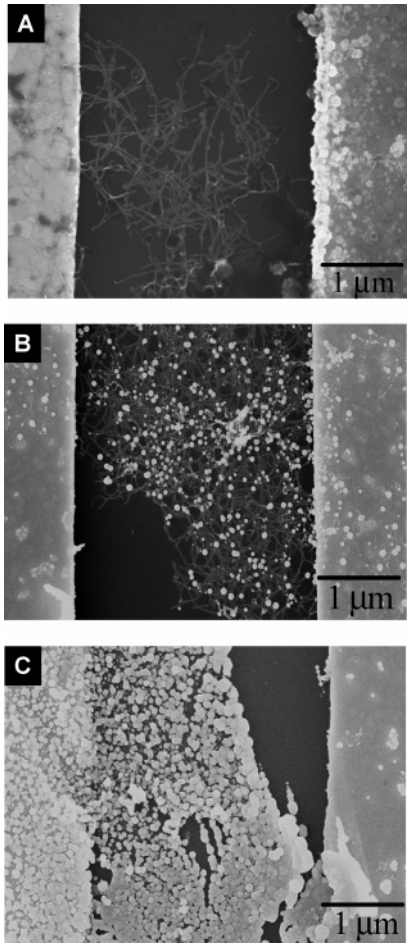


**Figure 4.** SEM image of bare SWNT before electrochemical functionalization (A) and (B) functionalization with Pd nanoparticles at 0.05 C and (C) 0.1 C.

size grew uniformly (Figure 3C) and began to coalesce with neighboring particles; as a result, a decreasing particle density trend was observed (Figure 3D). Figure 4 shows the SEM images of bare SWNTs and SWNTs decorated with Pd particles at different amount of charge passed keeping the potential constant at −0.8 V. At low deposition times (0.05 C), only a few Pd particles nucleate and grow on the SWNTs (Figure 4B). When the deposition time is increased (0.1 C), the size of the deposited metal nanoparticles uniformly increases resulting in a continuous film of Pd between the microelectrodes (Figure 4C). This illustrates that the electrodeposition method allows to precisely control the final size and nature of the metal deposits by varying the duration (i.e., the charge) of the deposition. In order to confirm that electrical conduction in the fabricated sensor is through SWNT network and that the electrodeposited Pd nanoparticles were non-continuous, electrical characterization of the sensors was performed. Room-temperature I−V characteristics show an S-shaped I−V curve for bare SWNTs and SWNTs decorated with a low density of Pd, while at increased Pd deposition time, an Ohmic behavior was observed (Figure 5A). For the low-density deposit case, temperature-resistance characteristics were also studied (Figure 5B). Resistance of the device increased with decrease in temperature indicating that current conduction path is through semiconducting SWNTs. By plotting ln $R$ versus $1/T$, the band gap energy of the Pd-decorated SWNTs sensor was calculated to be about 5 meV which is comparable to the band gap value of 6 meV obtained for bare SWNTs by Zhou et. al.[18]

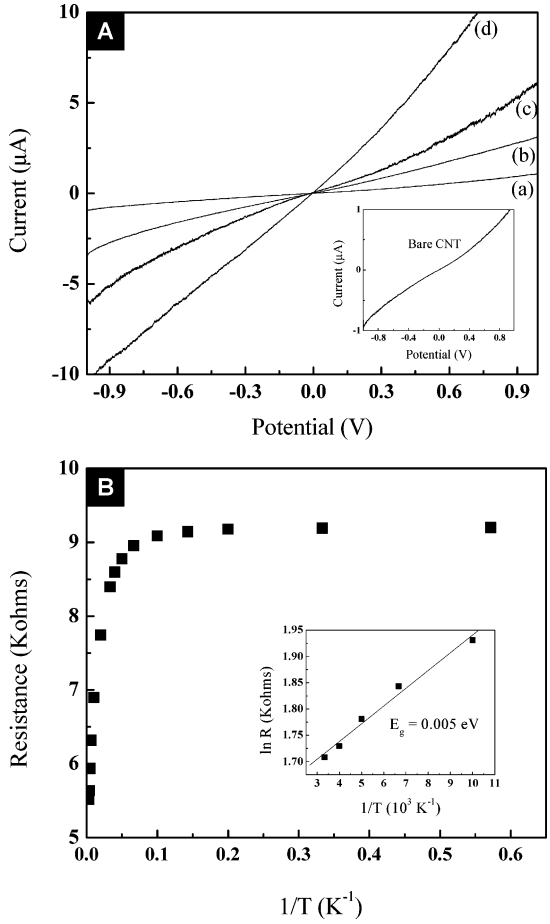


**Figure 5.** (A) I−V characteristics showing the resistance change with increase in amount of charge used for electrodeposition: (a) bare SWNTs, (b) Pd−SWNT with $C = 0.05$ C, (c) Pd−SWNT with $C = 0.08$ C, and (d) Pd−SWNT with $C = 0.1$ C. (B) Temperature-dependent resistance behavior of the sensor device fabricated at 0.05 C (error bars are smaller than the symbols). The inset is a plot of ln $R(T)$ vs $1/T$, showing a linear response. The slope is proportional the activation energy which is ∼0.005 eV. The scale of error bars was smaller than the scale of symbols.

The dynamic responses of two sensors with different Pd loading exposed to 200 ppm hydrogen in air are reported in Figure 6A. Within minutes of exposure to hydrogen, the resistance of the sensors increased to reach a steady value after 20 to 40 min. When, exposure to hydrogen ceased, the resistance slowly returned to its original value. The sensing mechanism for the Pd decorated SWNT sensor is based on the interactions between $H_2$, Pd, and SWNTs. The hydrogen atoms dissociate within Pd reaches the Pd−SWNT interface lowering its work function thereby allowing electrons to easily jump from Pd to SWNT. SWNTs being p-type material shows decrease in its conductance value because of the electron transfer from Pd−SWNT interface. The sensor response (defined as the change in resistance divided by the baseline resistance of the sensor in carrier gas) shows a significant decrease with increasing amount of Pd deposited. This was expected as Pd nanoparticles on SWNTs serve as nanogate electrodes and resistance tuning because of hydrogen adsorption depends upon the number of gate electrodes on SWNT. The greater the number of Pd nanoparticles on SWNT, the greater the magnitude in resistance change across SWNT, and the higher the response. As shown in Figure 3C and 3D, the number of Pd particles decreased with increasing deposition times. Hence, the response is much lower at longer deposition times where the current conduction is

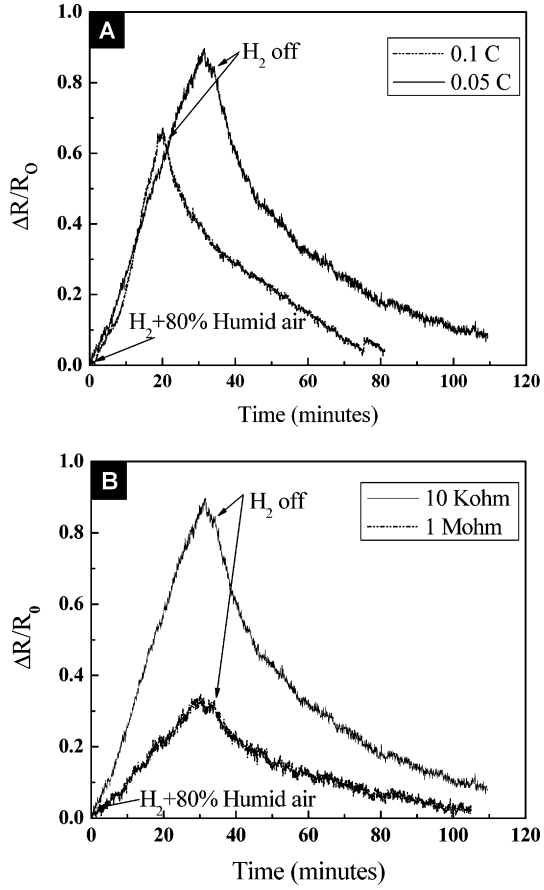


**Figure 6.** Sensor response to 200 ppm hydrogen in humid air for (A) different charges used for sensor synthesis (a) 0.05 and (b) 0.1 C and (B) different initial SWNT resistance (a) 10 KOhm and (b) 1 MOhm.

through a Pd film. We also investigated the effect of baseline resistance of SWNT network on sensing performance. We observed an increase in sensor response with decreasing baseline SWNT network resistance (Figure 6B). The optimal resistance was about 10 Kohm. This is consistent with the finding by Jing Li et al.[15] showing that when SWNT networks have a greater number of interconnects, a lower resistance is generally observed which results in increased available surface area for sensing applications and better sensing performance.

We also examined the carrier gas effect on responses of Pd−SWNT sensors to hydrogen. Three carrier gases—argon, dry air, and humid air (80%)—were selected to study the behavior of the Pd decorated SWNT sensors. All experiments were carried out at ambient conditions. As shown in Figure 7, in the case of dry air, the sensor showed a prompt resistance change upon exposure to hydrogen (400 ppm), however the time needed for complete recovery was large (>1 h). The presence of moisture in air did not markedly change the response after exposure to hydrogen, but it significantly shortened the recovery time. There was little or no recovery when the experiment was conducted in argon. The probable reactions that take place during hydrogen exposure and recovery stages have been proposed by Lundström et.al:[19]

$$H_{2,\text{ in air}} \leftrightarrow 2H_{\text{on Pd surface}} \leftrightarrow 2H_{\text{on Pd-SWNT interface}} \quad (1)$$

$$2H_{\text{on Pd surface}} + O_{2,\text{in air}} \leftrightarrow 2(OH)_{\text{on Pd surface}} \quad (2)$$

$$H_{\text{on Pd surface}} + (OH)_{\text{on Pd surface}} \leftrightarrow H_2O \quad (3)$$

Reaction 1 results in atomic hydrogen dissolved in the palladium, which can rapidly diffuse to the SWNT−Pd interface

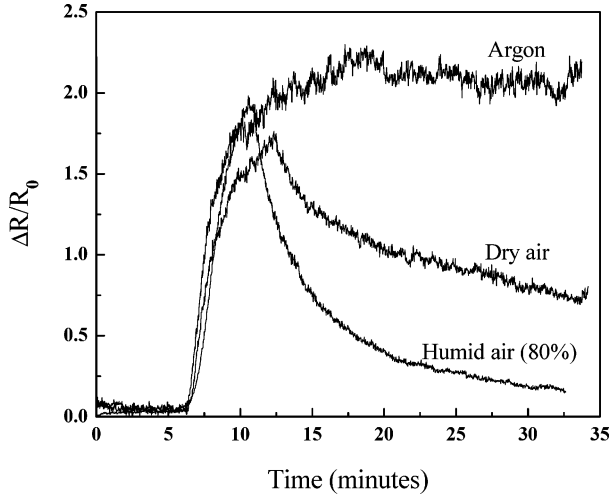


**Figure 7.** Sensor response to 400 ppm hydrogen for three different carrier gases.

and alter the electronic work function, thereby modulating the electrical resistance of the sensor assembly. When oxygen is present, dissolved oxygen can react with adsorbed atomic hydrogen to form hydroxyl groups (reaction 2) which will further react with adsorbed hydrogen to form water (reaction 3). Hence, the hydroxyl ions formed by the reaction of oxygen with hydrogen markedly accelerates the recovery of hydrogen. This is consistent with the faster recovery of the sensor in air and humid air versus argon reported in Figure 7. The exact mechanism underlying for the enhanced recovery in the presence of moist air is not yet completely understood. With humid air, one probable reaction is that the water vapor gets dissociated on the Pd surface giving rise to $H^+$ and $OH^-$ ions as shown in Reaction 4. The additional $OH^-$ ions from water vapor may react with the hydrogen inside the Pd surface resulting in faster recovery of hydrogen:

$$H_2O \leftrightarrow H^+ + (OH)^- \quad (4)$$

The response of a 10 Kohm Pd−SWNT sensor to hydrogen exposures (100 to 3000 ppm) in 80% relative humidity air at room temperature and ambient pressure is shown in Figure 8A. In each case, the sensor promptly reached a steady-state during exposure to hydrogen, and returned to its baseline when hydrogen feed was discontinued (see Figure 8A inset). The sensor showed a linear relationship for concentrations ranging from 100 to 1000 ppm (Figure 8B inset), and sensor saturation is evident above 3000 ppm. Our results shows that electrochemically functionalized CNT sensor showed a superior sensitivity (sensor response for the entire linear concentration regime) of about 0.4% per ppm hydrogen, far better than that observed by Kong et. al[10] and Sayago et.al.[20] which used vacuum evaporation and sputtering to functionalize SWNTs. We believe that this is because during electrochemical functionalization, the metal is deposited only on the defect sites which serve as a conduction barrier. The resistance is highly dependent on $H_2$−Pd interaction in these sites, hence the superior sensitivity compared to sensors made by metal evaporation or sputtering methods, where the entire surface of CNTs is coated. The lower detection limit of hydrogen was about 100 ppm. The response time, defined as the time required for the sensor to reach 90% of the final signal, did not vary much in the linear range of detection, but showed a rapid decrease at concentrations above 3000 ppm in the saturation regime

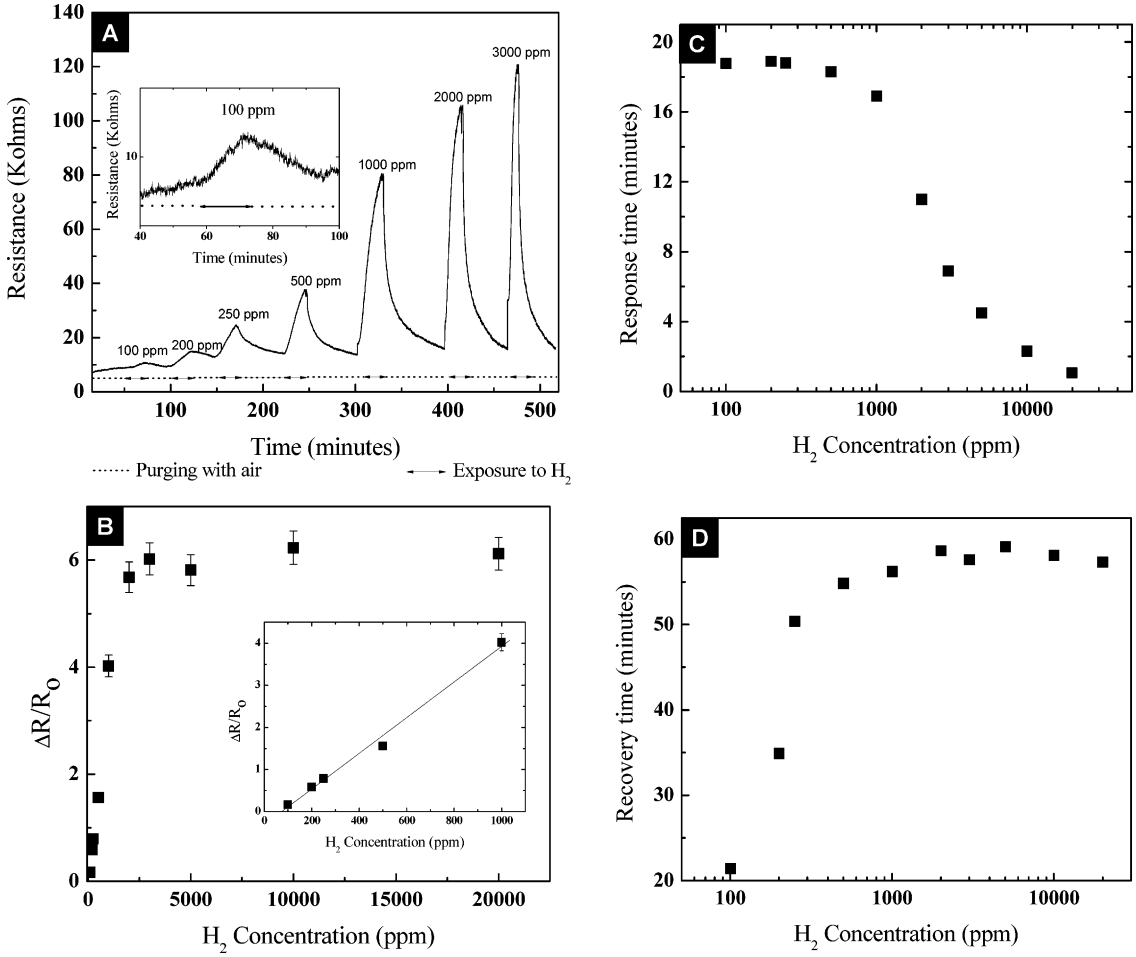


**Figure 8.** Sensor performance of (A) a 10 KOhm sensor (charge passed is 0.05 C) exposed to different concentrations of hydrogen in 80% relative humidity air. The inset is a magnification of the response to 100 ppm $H_2$. (B) Measured resistance change with respect to $H_2$ concentration. The linear response range of the sensor is shown in the inset. (C) Response time of the sensor and (D) recovery time as function of hydrogen concentration. The scale of error bars was smaller than the scale of symbols for some data points.

(Figure 8C). At room temperature, the response time was about 18 min for hydrogen concentrations up to 300 ppm and decreased to about 7 min at 3000 ppm. For higher concentrations in the saturation regime, the response time could be as short as 1 min. Complete recovery was observed for the sensors at all concentration range and recovery time varied from 20 min at 100 ppm to 55 min at 1000 ppm (Figure 8D).

## Conclusion

A hydrogen nanosensor working at room temperature was fabricated by electrodepositing palladium nanoparticles on SWNTs. Compared to other functionalization techniques; electrodeposition offers a simple, cost-effective, and site-specific way of decorating nanostructured materials. In order to improve the sensing performance, the Pd electrodeposition conditions (i.e., electrodeposition potential and charge) were optimized. The results demonstrated that the SWNTs could be functionalized with Pd ranging from nanoparticles to a thin film. Sensors with a baseline resistance of about 10 KOhm and deposition charge of 0.05 C at −0.8 V versus Ag/AgCl showed superior sensitivity (0.42%/ppm with a detection limit of 100 ppm) over other reported results. The recovery time of the sensor after exposure to hydrogen was greatly shortened when sensing was conducted in humid air. Since the desired material is electrodeposited directly on the sensing materials, we are currently investigating the use of this method to fabricate high density individually addressable nanosensor arrays depositing different materials. Such arrays will enable sensing of different analytes and discrimination of single compounds in gas mixtures on a single platform.

**Acknowledgment.** Funding for the project was provided by Bourns, Inc., University of California Discovery Grant (UC Discovery), and the Defense Microelectronic Activity (DMEA) under Agreement Number H94003-05-2-0505.

## References and Notes

(1) Grimes, C. A.; Ong, K. G.; Varghese, O. K.; Yang, X.; Mor1, G.; Paulose, M.; Dickey, E. C.; Ruan, C.; Pishko, M. V.; Kendig, J. W.; Mason, A. J. *Sensors* **2003**, *3*, 69−82.

(2) Cheng, C.; Tsai, Y.; Lin, K.; Chen, H.; Hsu, W.; Hung, C.; Liu, R. C.; Liu, W. *IEEE Sens. J.* **2006**, *6*, 287−292.

(3) Katsuki. A; Fukui, K. *Sens. Actuators, B* **1998**, *52*, 30−34.

(4) Berlin, C. W.; Sarma, D. H. R. Thick Film Sense Resistor Composition and Method of Using the Same. Delco Electronics Corp. U.S. Patent 5,221,644, June 22, 1993.

(5) Wolfe, D. B.; Love, J. C.; Paul, K. E.; Chabinyc, M. L.; Whitesides, G. M. *Appl. Phys. Lett.* **2002**, *80*, 2222−2224.

(6) Lundström, I.; Shivaraman, S.; Svensson, C.; Lundkvist, L. *Appl. Phys. Lett.* **1975**, *26*, 55−57.

(7) Dwivedi, D.; Dwivedi, R.; Srivastava, S. K. *Sens. Actuators, B* **2000**, *71*, 161−168.

(8) Im, Y.; Lee, C.; Vasquez, R. P.; Bangar, M. A.; Myung, N. V.; Menke, E. J.; Penner, R. M.; Yun, M. *Small* **2006**, *2*, 356−358.

(9) Favier, F.; Walter, E. C.; Zach, M. P.; Benter, T.; Penner, R. M. *Science* **2001**, *293*, 2227−2231.

(10) Kong, J.; Chapline, M. G.; Dai, H. *Adv. Mater.* **2001**, *13*, 1384−1386.

(11) Varghese, O. K.; Gong, D.; Paulose, M.; Ong, K. G.; Grimes, C. A. *Sens. Actuators, B* **2003**, *93*, 338−344.

(12) Krupke, R.; Hennrich, F.; Lohneysen, H. V.; Kappes, M. M. *Science* **2003**, *301*, 345−347.

(13) Qi, P.; Vermesh, O.; Grecu, M.; Javey, A.; Wang, Q.; Dai, H. *NanoLetters* **2003**, *3*, 347−351.

(14) Kong, J.; Franklin, N. R.; Zhou, C.; Chapline, M. G.; Peng, S.; Cho, K.; Dai, H. *Science* **2000**, *287*, 622−625.

(15) Li, J.; Lu, Y.; Ye, Q.; Cinke, M.; Han, J.; Meyyappan, M. *NanoLetters* **2003**, *3*, 929−933.

(16) Fan, Y.; Goldsmith, B. R.; Collins, P. J. *Nat. Mater.* **2005**, *4*, 906−911.

(17) Bangar, M. A.; Ramanathan, K.; Yun, M.; Lee, C.; Hangarter, C.; Myung, N. V. *Chem. Mater.* **2004**, *16*, 4955−4959.

(18) Zhou, C.; Kong, J.; Dai, H. *Phy. Rev. Lett.* **2000**, *84*, 5604−5607.

(19) Lundström, I.; Shivaraman, M. S.; Svensson, C. *Surf. Sci.* **1977**, *64*, 497−519.

(20) Sayagoa, I.; Terradob, E.; Lafuenteb,E.; Horrilloa, M. C.; Maserb,W. K.; Benitob, A. M.; Navarroc, R.; Urriolabeitiac, E. P.; Martinezb, M. T.; Gutierreza, J. *Synth. Met.* **2005**, *148*, 15−19.